Photoacoustics 40 (2024) 100651

Contents lists available at ScienceDirect

Photoacoustics

journal homepage: www.elsevier.com/locate/pacs

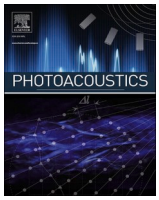

Photoacoustic thermal-strain measurement towards noninvasive and accurate temperature mapping in photothermal therapy

Zezheng Qin [a,b,c], Puxiang Lai [d,e,*], Mingjian Sun [a,b,c,**]

[a] Department of Control Science and Engineering, Harbin Institute of Technology, Harbin, Heilongjiang 150001,China
[b] Department of Control Science and Engineering, Harbin Institute of Technology, Weihai, Shandong 264200, China
[c] Harbin Institute of Technology Suzhou Research Institute, Suzhou, Jiangsu 215000, China
[d] Department of Biomedical Engineering, Hong Kong Polytechnic University, 999077, Hong Kong, China
[e] Shenzhen Research Institute, Hong Kong Polytechnic University, Shenzhen 518000, China

ARTICLE INFO

Keywords:
Photothermal therapy
Thermal strain
Photoacoustic imaging
Temperature imaging

ABSTRACT

Photothermal therapy is a promising tumor treatment approach that selectively eliminates cancer cells while assuring the survival of normal cells. It transforms light energy into thermal energy, making it gentle, targeted, and devoid of radiation. However, the efficacy of treatment is hampered by the absence of accurate and noninvasive temperature measurement method in the therapy. Therefore, there is a pressing demand for a noninvasive temperature measurement method that is real-time and accurate. This article presents one such attempt based on thermal strain photoacoustic (PA) temperature measurement. The method was first modelled, and a circular array-based photoacoustic photothermal system was developed. Experiments with Indian ink as tumor simulants suggest that the temperature monitoring in this work achieves a precision of down to 0.3 °C. Furthermore, it is possible to accomplish real-time temperature imaging, providing accurate two-dimensional temperature mapping for photothermal therapy. Experiments were also conducted on human fingers and nude mice, validating promising potentials of the proposed method for practical implementations.

1. Introduction

Photothermal therapy (PTT) is a therapeutic approach that uses materials with high photothermal conversion efficiency to selectively eliminate cancer cells without harming normal cells. The photothermal materials extensively studied in photothermal therapy encompass organic nano-photothermal conversion materials, precious metal nanoparticles, metal chalcogenide nanomaterials, and carbon-based photothermal conversion materials. These materials are injected into human body and accumulate near tumor sites actively or passively [1–4]. When exposed to optical illumination, these materials convert light energy into heat via absorption, raising the in-situ temperature above certain threshold, which could lead to cell disfunction or necrosis. As these materials only concentrate at and around the tumor sites, PTT can selectively kill cancer cells with minimal damage to surrounding healthy cells [5–7]. As seen, accurate monitoring of the in-situ temperature within tissue is crucial in PTT treatments, which, however, has not yet been implemented in most practices in the field [8]. Moreover, due to tissue diversity, there is need to adjust the strength and duration of laser illumination in PTT, which usually relies on prior knowledge or model-based estimation rather than real-time local temperature or treatment outcome feedback, which poses further challenges to achieve personalized treatment [9]. For example, in mild photothermal therapy (MPTT), the target treatment temperature must be maintained between 42°C and 45°C to eliminate cancer cells rapidly [10–12]. Therefore, to achieve precise PTT, high-precision and real-time temperature measurement is indispensable [13,14].

Currently, there are a many of invasive and cost-effective temperature monitoring approaches that could result in precise temperature measurement in PTT [15]. However, given the potential risk of tumor metastasis associated with wound formation, the use of such techniques is not ideal. The prevalent noninvasive temperature monitoring means employed in clinical settings encompass infrared temperature measurement, magnetic resonance (MR) temperature measurement, and ultrasound temperature measurement technology [16–18]. The infrared thermometer functions by detecting and quantifying the infrared

* Corresponding author at: Department of Biomedical Engineering, Hong Kong Polytechnic University, 999077, Hong Kong, China.
** Corresponding author at: Department of Control Science and Engineering, Harbin Institute of Technology, Harbin, Heilongjiang 150001,China.
E-mail addresses: puxiang.lai@polyu.edu.hk (P. Lai), sunmingjian@hit.edu.cn (M. Sun).

https://doi.org/10.1016/j.pacs.2024.100651
Received 2 July 2024; Received in revised form 6 September 2024; Accepted 18 September 2024
Available online 21 September 2024

radiation emitted by an object. The accuracy of infrared temperature monitoring is susceptible to external conditions and its capability is constrained by the penetration depth it supports due to strong scattering and absorption of near infrared light in tissue. Typically, it is recommended only for temperature measurements of the outer layer of the examined object but not for deeper tissue regions [19]. MR thermometry relies on the temperature-dependent shift of proton resonance frequency. Effective use of magnetic resonance temperature measurement necessitates the elimination of fat signals during imaging, and the equipment is costly and inaccessible for widespread adoption [20]. The core principle of ultrasonic temperature measurement involves evaluating the relationship between the velocity of ultrasonic waves and the temperature within a specific medium. For ultrasound-based temperature measurement means, although it offers relatively balanced performance between accuracy, penetration depth, and spatial resolution performance, attaining high-resolution temperature estimation in low echo tumor tissue proves challenging due to the internal acoustic properties of the tissue [21].

Photoacoustic effect is a phenomenon of material oscillation induced by the absorption of light energy. Imaging based on the photoacoustic effect, i.e., photoacoustic imaging, synergizes the benefits of optics and acoustics [22–27]. The contrast in ultrasound imaging is governed by the mechanical and elastic properties of the tissue, whereas in photoacoustic imaging, it is mainly determined by the optical properties, particularly optical absorption [28]. For instance, in breast cancer, the tumor region typically exhibits hypoechoic or anechoic characteristics, resulting in darkened areas on the ultrasound image. This suggests that the echo signals within the region are either abnormally weak or completely absent, thereby rendering this technology ineffective for temperature monitoring of specific areas during ultrasound imaging. Photoacoustic imaging is capable of visualizing light-absorbing substances, such as hemoglobin in cancerous tumors, which are excited to generate strong photoacoustic signals. This capability enables precise monitoring of the tumor's temperature based on photoacoustic signals throughout the entire heating process. Photoacoustic technology synergizes the deep tissue penetration capability of ultrasonic techniques with the high contrast resolution of optical methods, thereby enabling more precise tissue temperature measurements at specified depths and within defined spatial ranges. Photoacoustic temperature measurement leverages the inherent positive correlation between photoacoustic signals and localized thermal changes to estimate in-situ temperatures, offering the potential for non-invasive, precise, and real-time temperature monitoring in PTT. Especially, thermal strain temperature measurement is advantageous over regular amplitude-based photoacoustic temperature measurement means, as it substantially reduces the following factors that may affect the measurement results: inadequate stability of light-absorbing materials used in imaging targets, significant fluctuations in pulse laser energy, as well as the lack of a positive correlation between temperature and the Grueneisen coefficients of certain substances [29–32]. In this manuscript, we introduce a novel photoacoustic temperature measurement method based on thermal strain. This method operates independently of the photoacoustic signal amplitude, effectively eliminating the aforementioned interference factors associated with amplitude-based photoacoustic techniques, thereby providing a more precise and robust temperature monitoring approach in PTT. To confirm the effectiveness of the proposed approach, we carried out a sequence of validation trials, which include theoretical modelling and temperature measurement experiments with Indian ink tumor-mimicking phantoms, human fingers, and naked mice. All experimental results unequivocally showcase the capacity of the proposed method for robust temperature monitoring of a high level of precision, which could potentially generate widespread applications in PTT.

2. Methods and materials

This section outlines the techniques employed to acquire and examine the empirical findings of this study. At first, we provided a description of the photoacoustic temperature measuring and temperature imaging technique that relies on thermal strain. It also includes the necessary formulas for this technology. Next, we presented a detailed description of a circular-array photoacoustic computed tomography (PACT) system designed for temperature monitoring. The system's hardware components and operational logic were also explained. Finally, the different imaging targets and corresponding experimental settings used in this experiment were introduced: humanoid, nude mice, and human fingers.

3. Theoretical model

Assuming the initial temperature θ_0 in the tissue is uniformly distributed, and regardless of the time it takes for the pulsed laser to irradiate the tissue and convert it into sound pressure, if the initial time is T_0, the time delay for a photoacoustic signal from the axial depth a to reach the probe can be expressed as [33]:

$$t_c(a) = \int_0^a \frac{d\xi}{c(\xi, \theta(\xi))} \tag{1}$$

where $\theta(\xi) = \theta_0 + \delta\theta(\xi)$ is the temperature at the tissue depth, and $c(\xi, \theta(\xi))$ is the sound velocity in the tissue at depth ξ and temperature $\theta(\xi)$. Further considering the thermal expansion effect, when the temperature of the tissue whose axial size is $d\xi$ changes, its axial size changes to $(1 + \alpha(\xi)\delta\theta(\xi))d\xi$, where $\alpha(\xi)$ is the thermal expansion coefficient of the tissue at the depth of ξ, and Eq. (1) can be rewritten as:

$$t_c(a) = \int_0^a \frac{1 + \alpha(\xi)\delta\theta(\xi)}{c(\xi, \theta(\xi))} \cdot d\xi \tag{2}$$

Therefore, at the initial time $T_0 = 0$, the signal delay time is $t_0 = \int_0^a \frac{1}{c(\xi, \theta_0)} d\xi$. Once the temperature in the medium changes encompass both the surface and interior of the tissue, the time difference between the signal time delay and the initial signal time delay can be expressed as:

$$\delta t(a) = t(a) - t_0(a) = \int_0^a \left[\frac{1 + \alpha(\xi)\delta\theta(\xi)}{c(\xi, \theta(\xi))} - \frac{1}{c(\xi, \theta_0)} \right] d\xi \tag{3}$$

The axial differentiation of Eq. (3) can be obtained as:

$$\frac{\partial}{\partial a}(\delta t(a)) = \frac{1 + \alpha(a)\delta\theta(a)}{c(a, \theta(a))} - \frac{1}{c(a, \theta_0)} \tag{4}$$

In the photothermal therapy temperature range, the relationship between the speed of sound in the tissue and the temperature can be approximated as a linear relationship:

$$c(a, \theta(a)) = c_0(a)(1 + \beta(a)\delta\theta(a)) \tag{5}$$

where $\beta(a) = \frac{1}{c_0(a)} \cdot \frac{\partial c(a,\theta)}{\partial \theta}\Big|_{\theta=\theta_0}$ is the linear relationship coefficient between the tissue sound velocity and temperature, and $c_0(a) = c(a, \theta_0)$. So, according to Eq. (5), the time difference to depth differential can be rewritten as:

$$\begin{aligned} \frac{\partial}{\partial a}(\delta t(a)) &= \frac{1 + \alpha(a)\delta\theta(a)}{c_0(a)(1 + \beta(a)\delta\theta(a))} - \frac{1}{c_0(a)} \\ &= \frac{(\alpha(a) - \beta(a))\delta\theta(a)}{c_0(a)(1 + \beta(a)\delta\theta(a))} \end{aligned} \tag{6}$$

The change of the speed of sound due to temperature change can be approximately ignored as $|\beta(a)\delta\theta(a)| \ll 1$, and hence the relationship between temperature changes and time delay per unit length can be expressed by Eq. (6):

$$\delta\theta(a) = c_0(a)\left(\frac{1}{\alpha(a)-\beta(a)}\right)\cdot\frac{\partial}{\partial a}(\delta t(a)) \tag{7}$$

where $k(a) = 1/(\alpha(a)-\beta(a))$ is the material-related parameter, whose value can be calculated from the experiment of homogeneous material. Before temperature measurement, it is essential to calibrate k through experiment. The isovolumetric expansion coefficient has only a 0.01 % change under the unit temperature change, so the offset of the signal in time will be given by the variation of sound speed with temperature. The speed of sound is determined by the change of temperature, and the lateral deformation caused by the volume expansion coefficient has a negligible effect on the signal. Moreover,$c_0(a)\cdot(\partial\delta t(a)/\partial a)$ in Eq. (11) can be regarded as the comprehensive thermal strain variable of the sound velocity change due to the temperature change in the unit length [34–36].

Note that the signal offset of photoacoustic signals caused by temperature changes is typically negligible in practice. Therefore, the effective and accurate measurement of this signal offset plays a crucial role in determining the practicality of photoacoustic temperature estimation. A tenfold cubic spline interpolation to the original photoacoustic signal will be applied in this study and normalized cross-correlation will be utilized to determine the temporal offset of photoacoustic signals at various time points.

The above model is derived for the one-dimensional case, but it can also be extended to estimate temperature on a two-dimensional plane as follows. First, a set of 2-D RF data $r(a, x, T_0)$ are collected at the initial time before tissue heating, then the tissue is heated, and the RF data $r(a, x, T_i)$ is collected during the heating process. Select the photoacoustic signals at the same lateral position x_j and the same axial position a_k to a_{k+M}, a total of M+1 points whose spatial depth corresponds to the photoacoustic signals at the M+1 points is defined as the window size. Next, let the two signals be X_{j,k,T_0} and Y_{j,k,T_i} respectively, and then we perform cross-correlation analysis with a fixed window size from the starting point of the signal to obtain the time delay of the photoacoustic signal at different depths. Finally, axial differentiation is performed to convert the space of the generated thermal strain [37]. The flow chart of the thermal strain estimation is illustrated in Fig. 1.

Temperature information at various depths along the axis of each array element can be obtained using the model described above. Similar to the process used for reconstructing photoacoustic images, the temperature information derived from thermal strain is projected back to the relevant pixel coordinates in the target region based on the axial depth. The temperature map of the target area is then smoothed to produce the final result. Fig. 2 illustrates the signal processing flow of photoacoustic temperature estimation based on thermal strain.

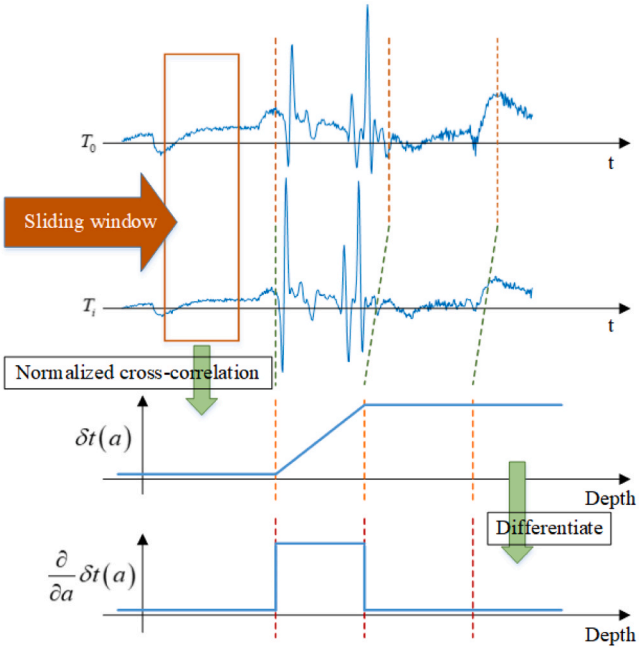

Fig. 1. Schematic diagram of thermal strain distribution estimation.

4. Circular-array photoacoustic photothermal system

The circular-array PTT system proposed in this work (Fig. 3) is constructed based on a programmable ultrasound imaging system (Prodigy, S-Sharp, Taiwan, China). The system primarily comprises four key modules: a photoacoustic signal excitation module, a continuous laser heating module, a signal receiving and processing module, and a temporal logic control module. The system can collect real-time photoacoustic signals and obtain temperature information of imaging targets based on the photoacoustic signals.

An optical parameter oscillation (OPO) pulsed laser with a multi-wavelength tunable function (SpitLight-600, Innolas, Munich, Germany) and a CW laser (LWIRL808–7 W-F, Laser, Beijing, China) at 808 nm wavelength were employed for PA signal excitation and target region heating, respectively. The circular-array probe comprises a semi-circular array with center frequencies of 2.5 MHz and 5.5 MHz. It features a scanning radius of 5.5 cm and consists of 256 array elements. The commercial ultrasound imaging platform (Prodigy, S-sharp, Taiwan, China) was used to receive and process the PA signals. To optimize the temperature measurement results, it is essential to regulate the collection of photoacoustic signals by monitoring the heartbeat of the living imaging target. The working sequence of the system based on the circular array is shown in Fig. 4. Note that the respiratory and cardiac motion of the living subject can alter the morphology and size of the imaging target. Consequently, it is crucial to maintain the target imaging region in a relatively stable position throughout each imaging and monitoring procedure to ensure accurate temperature measurements via thermal strain. Hence, in this work, the cardiac activity of the imaging subject was used as a stimulus signal to guarantee that the subject remained stationary during each imaging session.

On the other hand, in order to attain the onset and continuous monitoring of temperature change, the target area was routinely exposed to the CW laser. The nanosecond pulsed laser generates pulses of a width of 7 ns at a repetition rate of 20 Hz. The pulsed laser beam was coupled into a customized multimode fiber (Ceram Optec, Bonn, Germany), which was later divided into 8 paths to evenly distributed around the water tank to achieve annular illumination of the imaging target (Fig. 5). The water tank that held the phantom and tissue samples was made of acrylic material with a light transmittance of 98 %. In experiment, the CW laser heats the tumor phantom, and the temperature information is obtained in real time by a thermocouple in addition to PA measurement.

5. Sample preparation and arrangement

To assess the system's ability to measure temperature, we fabricated a tumor phantom with Indian ink. The tumor phantom was created by dissolving 2 g of Agar and 1 g of Gelatine in 94.5 ml of water to form the matrix of the phantom. Additionally, 1 g of corn starch were added to mimic sound scattering, and 1.5 g of Indian ink were added to represent the optical absorption of blood. The laser pulses at 532 nm were selected to generate photoacoustic signals, and the CW laser was positioned at the upper part of the phantom to provide uninterrupted irradiation and heating. After that, a thermocouple was inserted into the phantom to measure the in-situ temperature in real time.

To further verify the feasibility of the proposed system, experiments were also performed based on nude mice. This time, the photoacoustic signals were excited by 1064 nm laser pulses to allow for better penetration depth into tissue. We measured the laser energy distribution

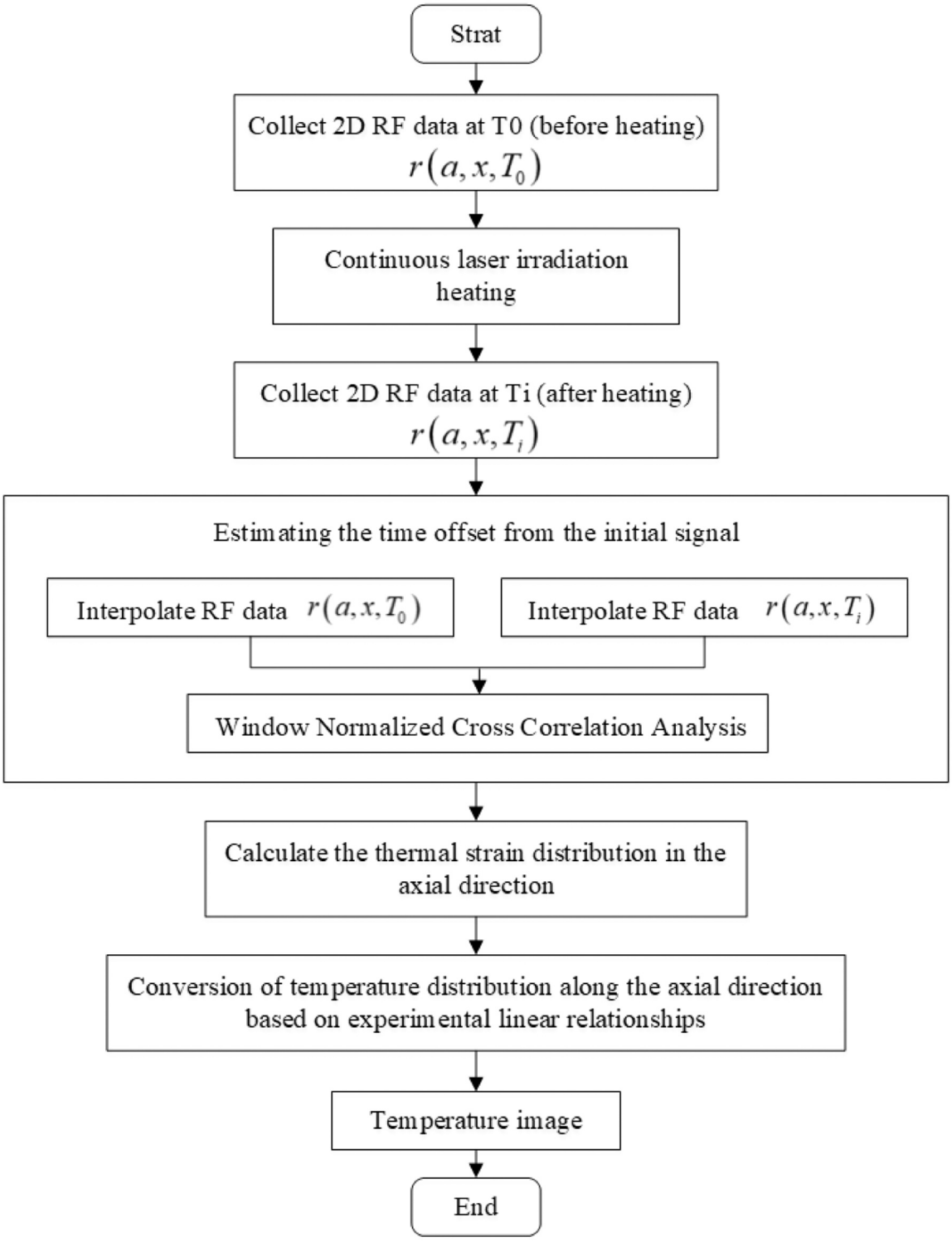

Fig. 2. The signal processing flow of photoacoustic temperature estimation based on thermal strain.

density of the tissue specimen to be 30 mJ/cm^2, which conforms to the ANSI safety standard. The heating laser was the same as the one used in the phantom study. By utilizing a gradual heating technique in mice, the temperature of the specific region is prevented from rising rapidly, taking approximately 10 minutes to reach its peak. During the experiment, each mouse was first anesthetized by vaporized isoflurane (1 L/min of air and 0.75 % isoflurane) with a small animal anesthesia system (R500IP, RWD, China). Then the anaesthetized mouse was secured on a home-built animal holder (Fig. 6b). Deionized water was utilized as the medium for acoustic coupling, and a moderate water temperature was maintained to prevent mouse death caused by hypothermia. Following the completion of all experiments, the mice were terminated using the cervical dislocation method. The experimental setup of naked mouse photoacoustic temperature measurement is shown in the following figure.

After that, we further conducted verifications based on human fingers. Similar parameters were adopted as for the animal experiments, also include that additional temperature measurement based on a digital

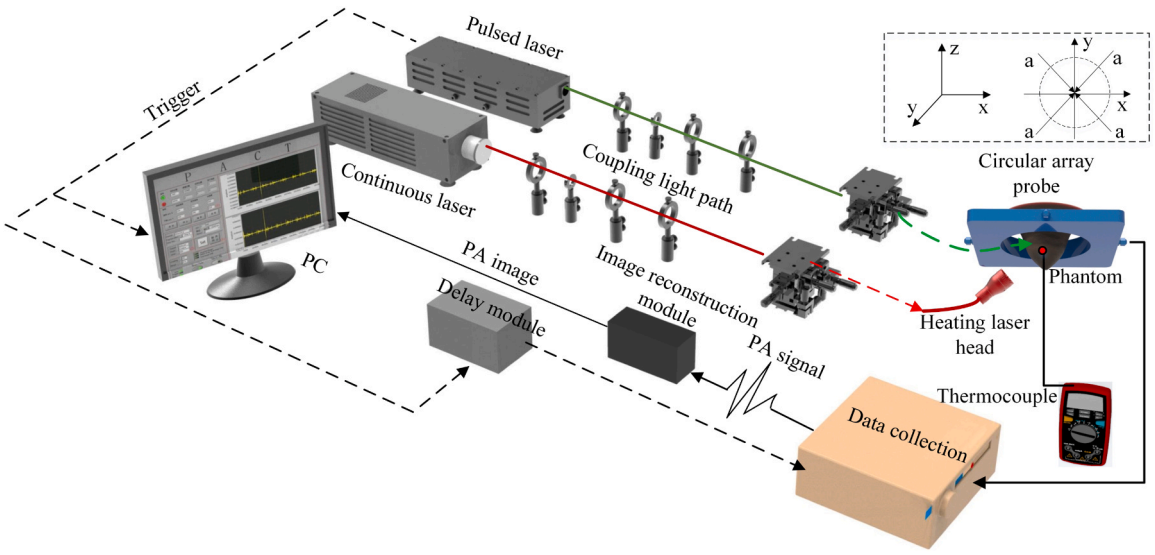

Fig. 3. Schematic diagram of the ring-array photoacoustic temperature monitoring system.

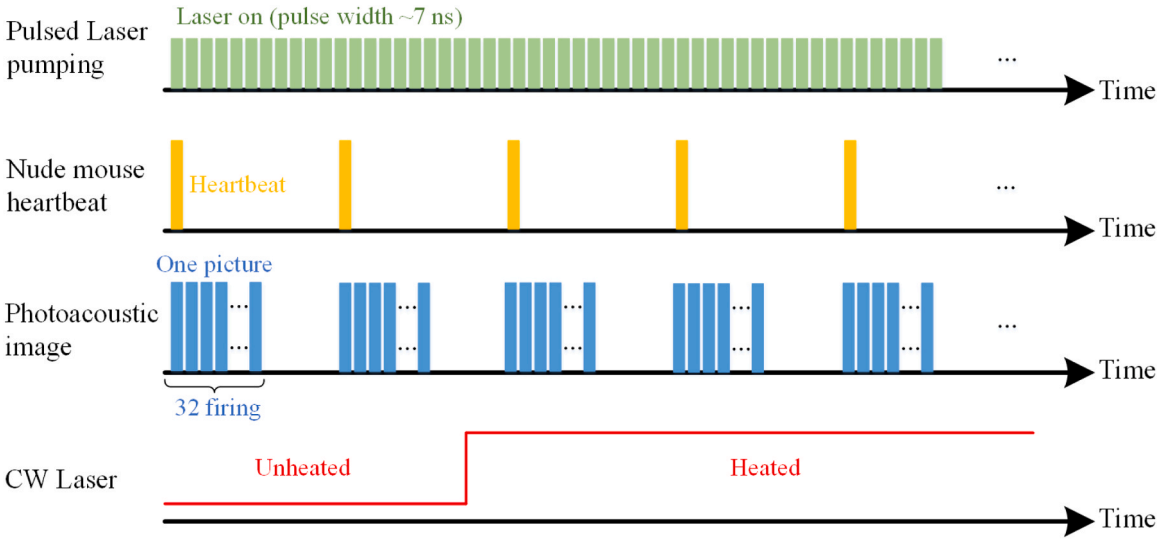

Fig. 4. Time base and synchronization of the laser heating and PA imaging modules.

thermometer (UT321, LINI-T, China) attached to the surface of mice and figure skin was arranged (Fig. 6c-d). During the experiment, the internal tissue temperature was approximated by correlating the skin surface temperature with the light attenuation and thermal conductivity properties of the biological tissue. The heating strength of the CW illumination was controlled to ensure that the temperature of the finger region was below 43 ℃. On the other hand, the heating period in experiment was kept short to avoid potential overheating to the finger skin.

6. Results

6.1. Photoacoustic temperature measurement based on tissue-mimicking phantoms

Experiments were first conducted based on tissue mimicking phantoms to establish correlation between the delay in flight time of photoacoustic signals with the measured in-situ temperature. Fig. 7a shows a photo of the phantom that contained an Indian ink-based absorbing target at the center. The local temperature of at the absorber was measured via an embedded thermocouple. As Indian ink exhibits a significant capacity to absorb light and results in robust photoacoustic signals at the boundaries of the absorber, regular amplitude-based photoacoustic image, as shown in Fig. 7b, provides a comprehensive representation of the overall shape and structure of the absorbing target.

The initial temperature is 20 ℃. Then the CW laser radiation was turned on to gradually raise the target temperature up to 50 °C to effectively cover the PTT temperature window, as monitored by the thermocouple. To achieve precise reconstruction of the temperature information based on photoacoustic signals, it is necessary to analyze the photoacoustic signals obtained from each individual element from the transducer array. As an illustrative example, we analyze the photoacoustic signal collected by the central element of the half-ring array on the corresponding side of the heated area to determine whether a linear correlation exists between the photoacoustic signal delay and temperature. To ensure the reliability of correlation, the measurements were repeated 10 times, as shown in Fig. 8, where the error bars represent the standard deviation of measurements. As seen, the time delay of photoacoustic signals increases overall linearly with the local temperature except when the temperature approaches or even goes beyond 50 °C, which could be attributed to the partial melting of the

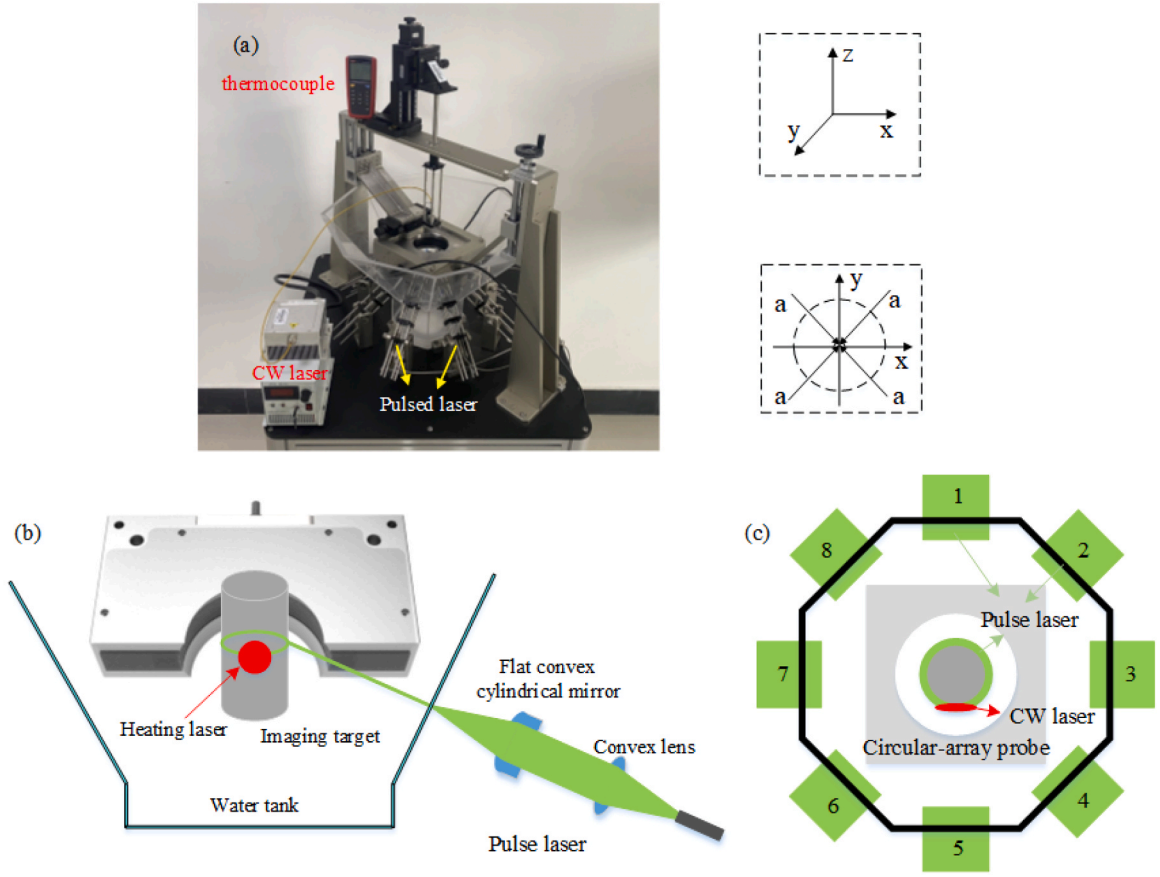

Fig. 5. Illustration of the laser heating and PA signal excitation arrangements: (a) overall hardware of the experiment; (b) front view; (c) side view.

matrix and target materials under intensive heating. Nonetheless, a linear fit could be applied for regimes well below the melting temperature. With this linear correlation, it is possible to predict the in-situ temperature within tissues from photoacoustic signals that are remote and noninvasive even without an embedded thermocouple.

Built upon this basis, we utilized thermal strain to derive the temperature distribution of the designated region based on the signal time delay. Specifically, the axial distribution of thermal strain of the PA signals collected by all 256 elements of the ring array transducer is obtained using the model proposed in this article, and then the image reconstruction algorithm is adopted to back project the temperature information to the region of interest. Fig. 9 shows an example of photoacoustic temperature image reconstructed based on photoacoustic signals when the target was heated up to 50 ℃ (as measured by thermocouples). As shown in the figure, the photoacoustic temperature image based on thermal strain accurately estimates the target temperature measured by thermocouples. Such a capability was further confirmed when the phantom sample was gradually heated by the CW laser from 25 to 50 ℃ and then cooled down back to the base temperature when the laser radiation was turned off (Fig. 10).

6.2. *Photoacoustic temperature measurement based on tissue samples in vivo*

After validation on tissue-mimicking phantoms, the study proceeded to in-vivo tissue samples. First, we performed regular photoacoustic imaging and temperature imaging on the mice's trunk, revealing details such as skin, blood arteries, vertebrae, and internal organs. Temperature image can offer insights on the spatial distribution of temperature in the heated region of mice. The mouse abdomen had an initial surface temperature of 30.9 ℃. Following prolonged exposure to laser radiation, the temperature ultimately increased to 42.4 ℃, which can also be predicted based on the photoacoustic temperature image as shown in Fig. 11b. To visually represent the temperature distribution with respect to tissue structures, we could overlay the two images into a fused one (Fig. 11c). To showcase our method's capability under different conditions, similar to phantom experiments, the temperature of the region of interest was gradually raised from 33.8 ℃ to 38.2 ℃ and then to 41.6 ℃, as measured by the thermocouple. The corresponding photoacoustic temperature images are shown in Fig. 11d-f, respectively. The 1D profiles across the dashed lines are shown in Fig. 11g, revealing peak temperatures of approximately 34.1 ℃, 38.4 ℃, and 41.9 ℃, respectively, being very close to the actual local temperatures.

Then, the study was extended to human subjects to further verify the efficacy of the method in more clinical scenes. The experimental settings were similar to those for live animal experiments, except that an adult human finger as depicted in Fig. 6 was used as the experiment subject in vivo. The initial temperature at the finger surface was 30 ℃ as measured by the thermocouple, which gradually increased up to 41.6 ℃ under the CW laser radiation to mimic the PTT application scenario. We obtained regular photoacoustic images, the corresponding photoacoustic temperature images, and an overlaying version of them, as exampled in Fig. 12a-c. As seen, the photoacoustic image depicts the spatial arrangement of blood vessels in the epidermis and subcutaneous layers of the human finger, whereas the temperature image shows the distribution of temperature in the heated region. Moreover, similar to the animal study, three photoacoustic temperature images were exampled when the finger surface temperature as measured by the thermocouple was 33.2 ℃, 36.1 ℃, and 41.6 ℃, respectively (Fig. 12d-f). Analysis of the profiles along the dashed lines (Fig. 12g) demonstrated that photoacoustic temperature measurements closely matched the thermocouple measurements, which are considered the ground truth in this study.

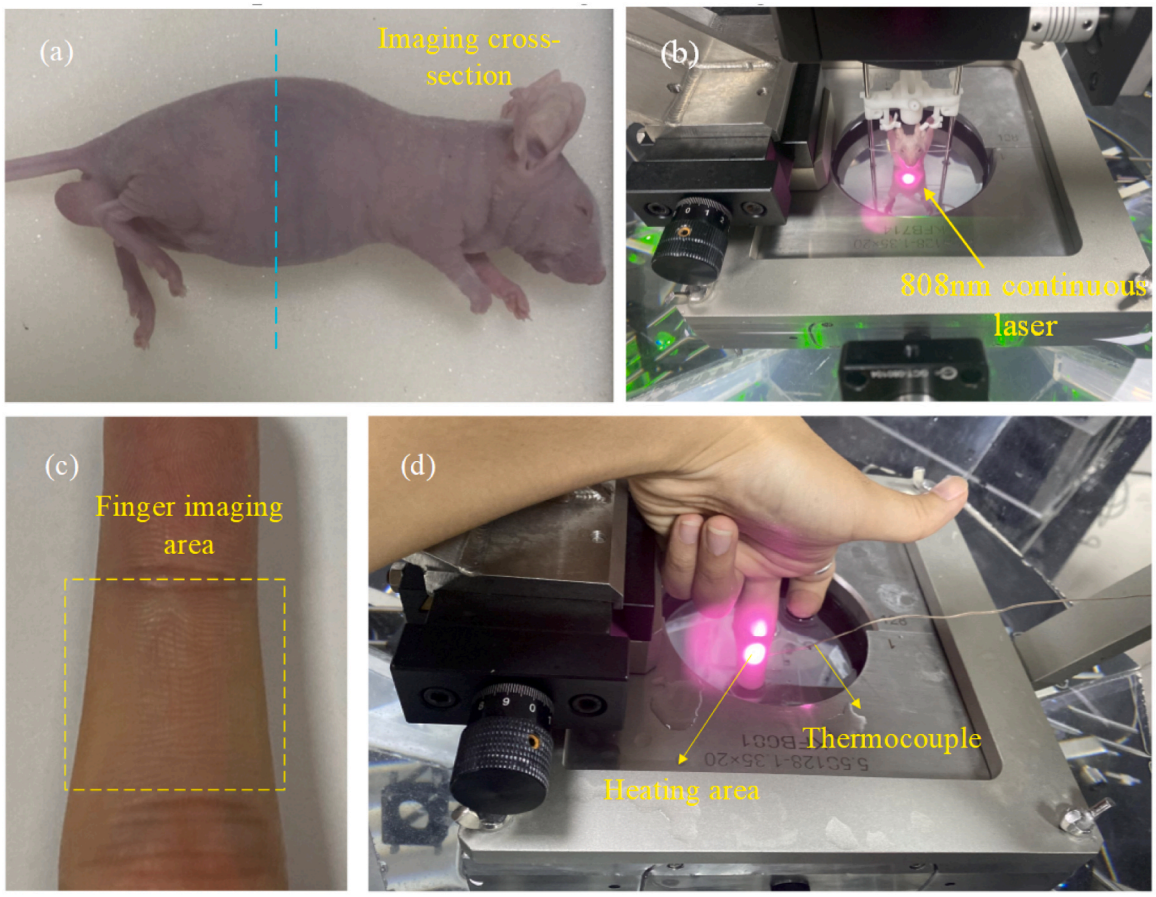

Fig. 6. Nude mouse and finger photothermal experiment: (a) live nude mouse after anesthesia; (b) positioning of the nude mouse with respect to the animal holder and the CW heating laser beam; (c) human finger; (d) experimental process settings.

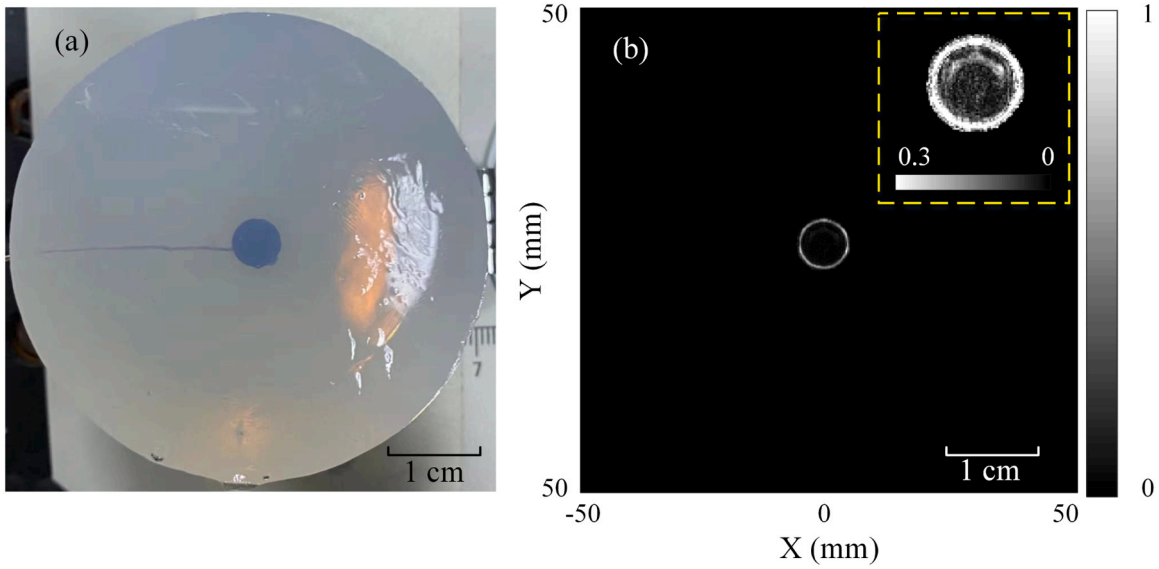

Fig. 7. Photograph of the tissue-mimicking phantom (94.5 % water; 2 % Agar; 1.5 % Indian ink; 1 % Gelatine; 1 % corn starch) (a) and its regular photoacoustic image (b).

7. Discussion

PTT is an innovative and noninvasive approach for treating malignant tumors that has gained prominence in recent times. It holds potential to supplant conventional methods like radiotherapy and chemotherapy in the treatment of cancer growth. During the procedure, a near-infrared laser beam illuminates the region of interest and raises the tissue temperature locally due to absorption, which triggers the programmed death of cancer cells, known as apoptosis. Precise temperature monitoring and visualization of the process are crucial to assure

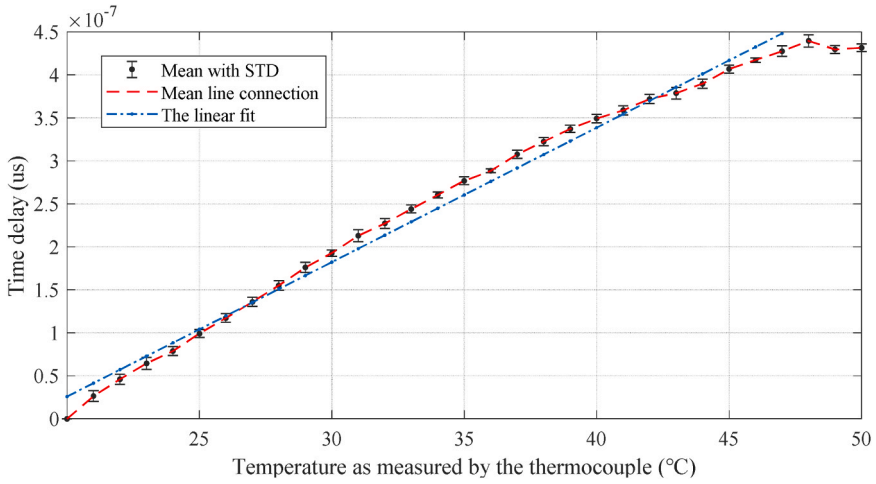

Fig. 8. The mean standard deviation image of 10 temperature measurement experiments.

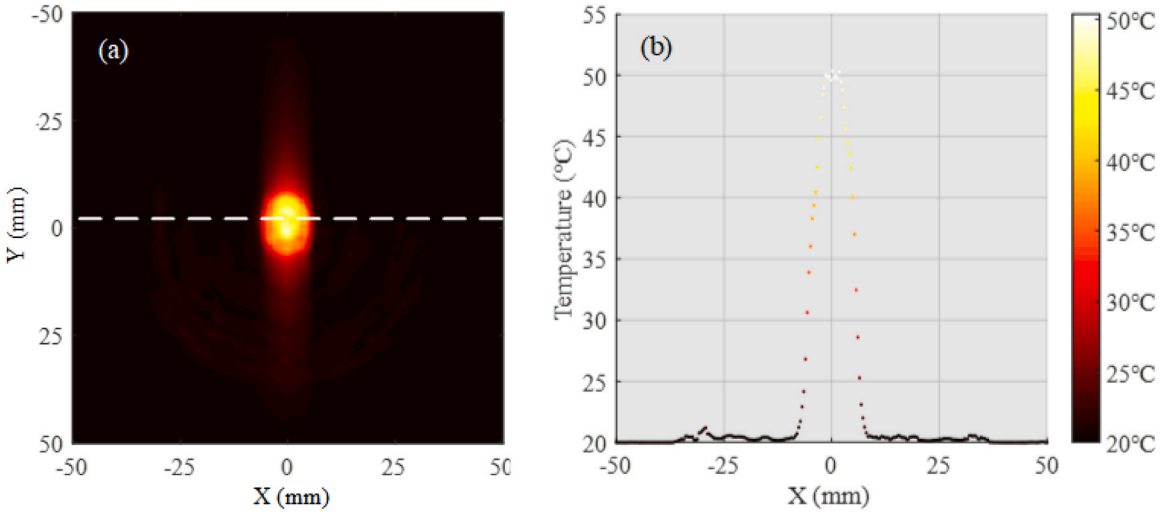

Fig. 9. An example photoacoustic temperature image (a) and the temperature distribution along the white dotted line (b).

the therapeutic effect while minimize damage to the surrounding normal tissues. Quite a few approaches have been proposed for temperature monitoring during PTT, yet all have their drawbacks [14]. For example, the precision of photoacoustic temperature measurement based on the Grueneisen effect is usually influenced by factors such as the variation of laser pulse energy, the stability of photothermal properties in the region of interest, as well as the dependence of the tissue's Grueneisen coefficient on temperature.

In this work, we start with the fact that in PTT, the variation of local temperature induces changes to the velocity of ultrasonic transmission, which would lead to a temporal shift of the generated photoacoustic signals under pulsed laser illumination. Built upon this phenomenon, the concept of measuring thermal strain temperature based on photoacoustic signals is proposed and modelled in this study. As this method relies on thermal strain and effectively circumvents the impact of factors discussed in the last paragraph, accurate temperature measurement based on the delay of photoacoustic signals becomes feasible, as validated through tissue-mimicking phantoms and live tissue experiments in this study. Throughout the research process, we constructed multiple phantom models to validate the algorithm, with the temperature measurements consistently demonstrating the algorithm's efficacy. The temperature measurement experiments conducted on two nude mice yielded accurate results, and further experimental validation was performed with the participation of a human volunteer. The dark regions observed in in-vivo photoacoustic images represent areas where the photoacoustic signal is either absent or only weakly excited. To achieve precise temperature monitoring in these regions, it is essential to enhance the excitation intensity of the photoacoustic signals within these areas. By increasing laser energy, or by modulating/shaping the diffused laser illumination [38–40], it is possible to penetrate deeper tissues to excite sufficient photoacoustic signals, thereby enabling reliable temperature monitoring in these regions. Additionally, photoacoustic dyes can be utilized to target specific regions, enhancing light absorption, which in turn enhances the photoacoustic signals and facilitates effective temperature monitoring within these regions.

That said, it should be noted that the accuracy of temperature measurement based on the proposed method might be significantly influenced due to the deformation of target region resulting from physiological motions like breathing and heartbeat of the live subjects. To avoid that effect, the subject's respiration and cardiac activity are employed as a stimulus indicator to maintain the target region's stability throughout each imaging session. Further attempts to reduce the influence of motion anomalies on temperature measurement will be implemented in the next phase of study such as utilizing laser pulses with higher repetition rates and developing an intelligent temperature control algorithm to establish a closed-loop control state. In this study, it is postulated that the temperature monitoring region comprises homogeneous and uniform tissue. A collimated continuous laser beam is

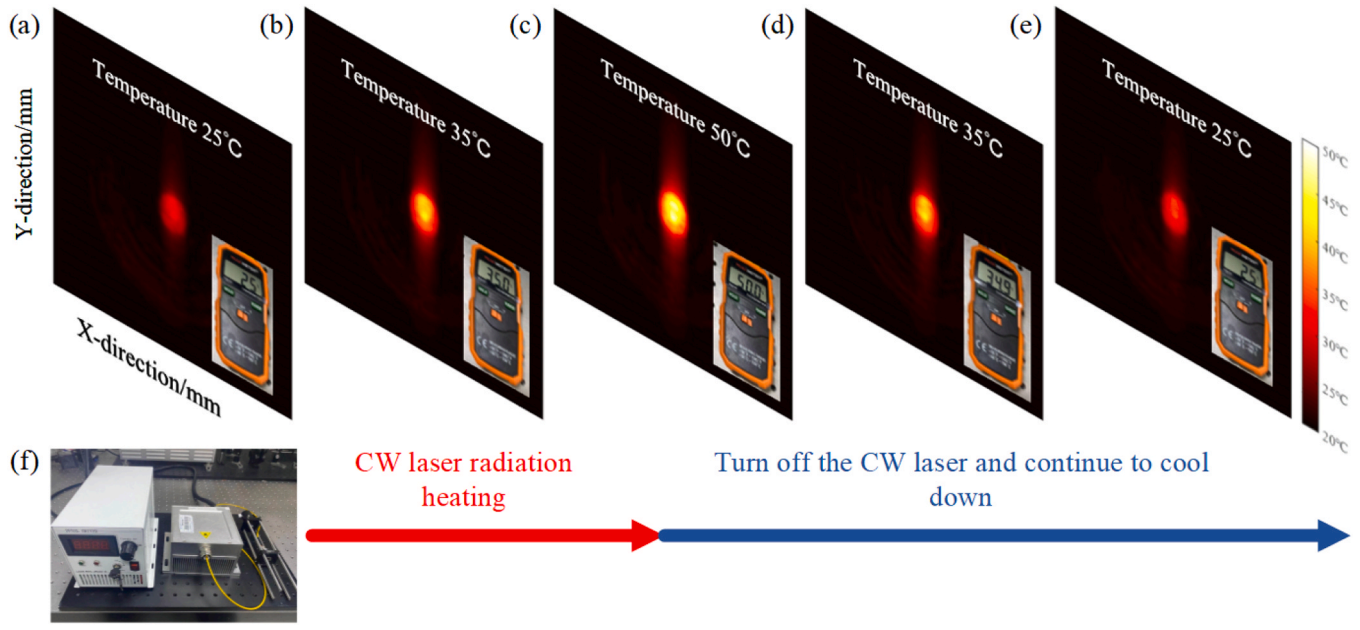

Fig. 10. Temperature images based on thermal strain at different temperatures: (a) 25 ℃ temperature image during heating process; (b) 35 ℃ temperature image during heating process; (c) 50 ℃ temperature image during heating process; (d) 35 ℃ temperature image during cooling process; (e) 25 ℃ temperature image during cooling process; (f) CW laser.

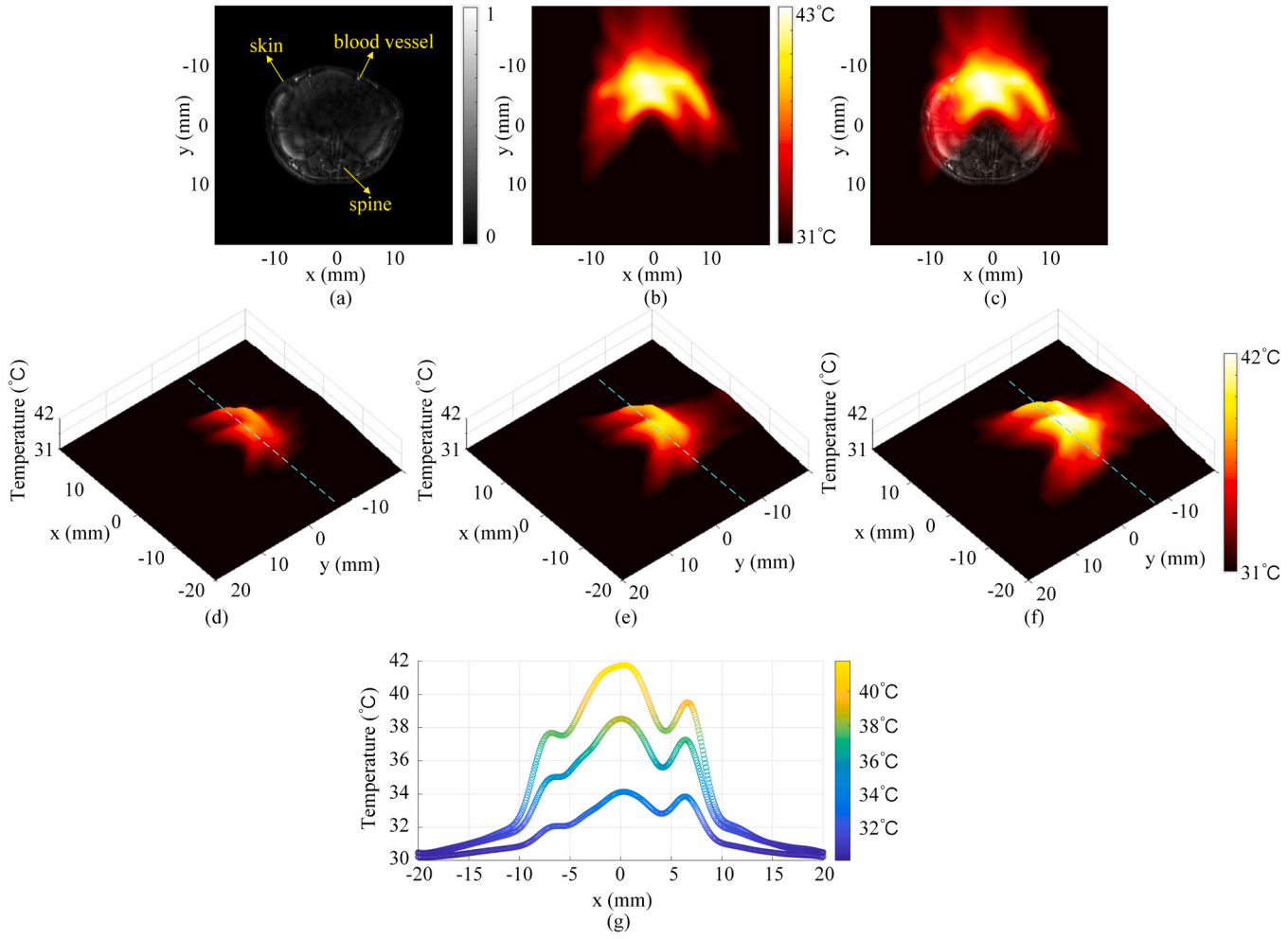

Fig. 11. Nude mouse photoacoustic and temperature imaging: (a) photoacoustic image; (b) temperature image at 42.4 ℃; (c) bimodal fusion image; (d)-(f) Temperature images at 33.8, 38.2, and 41.6 ℃, respectively; (g) Temperature distribution profiles along the dashed lines in (d)-(f).

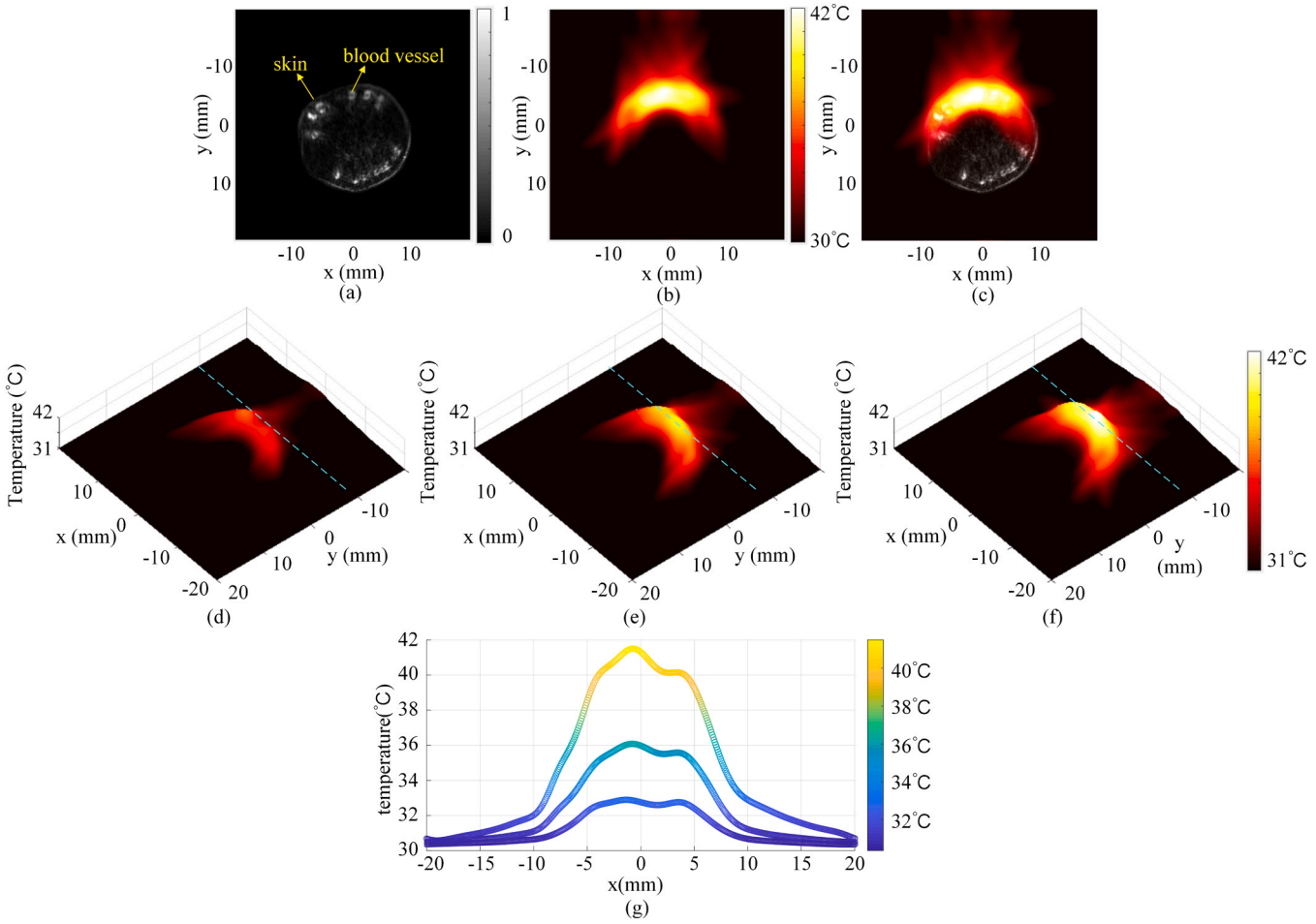

Fig. 12. Finger photoacoustic and temperature imaging: (a) photoacoustic image; (b) temperature image at 42.4 ℃; (c) bimodal fusion image; (d)-(f) Temperature images at 33.2, 38.2, and 41.6 ℃, respectively; (g) Temperature distribution profiles along the dashed lines in (d)-(f).

employed to irradiate and heat the target region. Taking into account the scattering and thermal conductivity properties of the tissue under laser irradiation, we multiply the skin surface temperature, as measured by the thermocouple, by the attenuation coefficient to derive the internal tissue temperature, subsequently determining the linear correlation coefficient between internal tissue thermal strain and temperature. In future work, the thermocouple-based temperature measurement method will be supplanted during the calibration process by more advanced temperature measurement technologies capable of precisely determining the internal temperature of the tissue. Concurrently, we are developing a comprehensive database, grounded in extensive experimental studies, to derive the linear correlation between thermal strain and temperature across various tissue types, and hence optimizing temperature monitoring. The algorithm proposed in this study demonstrates high accuracy in temperature monitoring. However, the spatial resolution of temperature imaging sees constrains. Currently, there is no established metric to quantify the resolution of temperature images generated in this study. When utilizing photoacoustic signals to assess the axial distribution of thermal strain, the resolution of temperature images diminishes as the window size increases in the sliding window technique. Furthermore, applying smoothing processes in temperature imaging can result in reduced spatial resolution of the imaging outcomes. To mitigate computational complexity, we have temporarily implemented a sliding window design featuring a fixed 200 sampling points and a 60 % overlapping rate. Future research will pay attention to determining the optimal sliding window configuration and other parameters to enhance the spatial resolution of temperature imaging. The correlation between thermal strain-induced temporal photoacoustic shifts and local temperature forms the foundation of accurate temperature measurement in this study.

8. Conclusion

This article introduces a photoacoustic temperature measurement and temperature imaging method that utilizes thermal strain. This method allows for accurate temperature monitoring during photothermal therapy and real-time visualization of the temperature distribution. It also helps guide the target temperature to stay within the optimal treatment temperature range. Thermal strain-based temperature measurement methods enhance temperature accuracy and minimize the impact of various interferences, in contrast to temperature measurement methods that depend on Grueneisen coefficients. Experimental study and theoretical analysis have revealed that the temperature measuring algorithm suggested in this article is vulnerable to the impact of respiratory and other movement displacements during in vivo studies. Throughout the experiment, we executed appropriate procedures to mitigate the influence of respiratory and cardiac motions on the temperature assessment of the subjects involved in the study. By conducting simulation and in vivo experimental study, it has been demonstrated that the temperature measurement method and system suggested in this paper may attain a temperature measurement accuracy of 0.3 ℃. Furthermore, they exhibit significant promise for utilization in human photothermal therapy.

CRediT authorship contribution statement

Puxiang Lai: Writing – review & editing. **Mingjian Sun:** Writing – review & editing. **Qin Zezheng:** Writing – original draft.

Declaration of Competing Interest

The authors declare that they have no known competing financial interests or personal relationships that could have appeared to influence the work reported in this paper.

Data availability

Data will be made available on request.

Acknowledgements

The research is supported by the National Key R&D Program of China [Grant No. 2023YFF0713600], the National Natural Science Foundation of China [Grant No. 62275062, 81930048], Project of Shandong Innovation and Startup Community of High-end Medical Apparatus and Instruments [Grant No. 2021-SGTTXM-005], the Shandong Province Technology Innovation Guidance Plan (Central Leading Local Science and Technology Development Fund) [Grant No. YDZX2023115], the Taishan Scholar Special Funding Project of Shandong Province, and the Shandong Laboratory of Advanced Biomaterials and Medical Devices in Weihai [Grant No. ZL202402].

References

[1] L. Xu, L. Cheng, C. Wang, et al., Conjugated polymers for photothermal therapy of cancer, Polym. Chem. 5 (5) (2014) 1573–1580.
[2] L. Huang, Y. Li, Y. Du, et al., Mild photothermal therapy potentiates anti-PD-L1 treatment for immunologically cold tumors via an all-in-one and all-in-control strategy, Nat. Commun. 10 (1) (2019) 1–15.
[3] X. Li, J.F. Lovell, J. Yoon, et al., Clinical development and potential of photothermal and photodynamic therapies for cancer, Nat. Rev. Clin. Oncol. 17 (11) (2020) 657–674.
[4] X. Huang, H. Hui, W. Shang, et al., Deep penetrating and sensitive targeted magnetic particle imaging and photothermal therapy of early-stage glioblastoma based on a biomimetic nanoplatform, Adv. Sci. 10 (19) (2023) 2300854.
[5] Y. Ma, Y. Liu, Z. Lei, et al., Multi-wavelength photoacoustic temperature feedback based photothermal therapy method and system, Pharmaceutics 15 (2) (2023) 555.
[6] W. Li, J. Yang, L. Luo, et al., Targeting photodynamic and photothermal therapy to the endoplasmic reticulum enhances immunogenic cancer cell death, Nat. Commun. 10 (1) (2019) 1–16.
[7] Y. Ma, Y. Liu, Z. Qin, et al., Mild-temperature photothermal treatment method and system based on photoacoustic temperature measurement and control, Biomed. Signal. Process. Control 79 (2023) 104056.
[8] D. Yeager, Y.S. Chen, S. Litovsky, et al., Intravascular photoacoustics for image-guidance and temperature monitoring during plasmonic photothermal therapy of atherosclerotic plaques: a feasibility study, Theranostics 4 (1) (2014) 36.
[9] N. Velpula, D.K. Maloth, S. Kodangal, et al., Photodynamic therapy: a new modality treatment in pre- cancer and cancer patients, Int. J. Case Rep. Images 5 (4) (2020) 250–257.
[10] Y. Ma, Z. Lei, D. Wu, et al., A neural network estimation model based light dose control method and system for low-temperature photothermal therapy, Biomed. Signal. Process. Control 85 (2023) 104935.
[11] X. Huang, P.K. Jain, I.H. El-Sayed, et al., Plasmonic photothermal therapy (PPTT) using gold nanoparticles, Lasers Med. Sci. 23 (3) (2008) 217–228.
[12] L.V. Wang, S. Hu, Photoacoustic tomography: in vivo imaging from organelles to organs, Science 335 (6075) (2012) 1458–1462.
[13] J. Shah, S. Park, S.R. Aglyamov, et al., Photoacoustic imaging and temperature measurement for photothermal cancer therapy, J. Biomed. Opt. 13 (3) (2008) 034024.
[14] C.H. Seo, Y. Shi, S.W. Huang, et al., Thermal strain imaging: a review, Interface Focus 1 (4) (2011) 649–664.
[15] Y. Ma, Y. Liu, Z. Qin, et al., Mild-temperature photothermal treatment method and system based on photoacoustic temperature measurement and control, Biomed. Signal Process. Control 79 (2023) 104056.
[16] S.W. Huang, K. Kim, R.S. Witte, et al., Inducing and imaging thermal strain using a single ultrasound linear array, IEEE Trans. Ultrason. Ferroelectr. Freq. Control 54 (9) (2007) 1718–1719.
[17] L. Li, L.V. Wang, Recent advances in photoacoustic tomography, BME Front. 2021 (1) (2021) 27, 2.
[18] L.V. Wang, Prospects of photoacoustic tomography, Med. Phys. 35 (12) (2008) 5758–5767.
[19] M. Pramanik, L.V. Wang, Thermoacoustic and photoacoustic sensing of temperature, J. Biomed. Opt. 14 (5) (2009) 054024.
[20] Wang S.H., Wei C.W., Jee S.H., et al. Photoacoustic temperature measurements for monitoring of thermal therapy[C]//Photons Plus Ultrasound: Imaging And Sensing 2009. International Society for Optics and Photonics, 2009, 7177: 71771S.
[21] F. Xiaohua, G. Fei, Z. Yuanjin, Photoacoustic-based-close-loop temperature control for nanoparticle hyperthermia, IEEE Trans. Biomed. Eng. 62 (7) (2015) 1728–1737.
[22] K. Kuroda, A.H. Chung, K. Hynynen, et al., Calibration of water proton chemical shift with temperature for noninvasive temperature imaging during focused ultrasound surgery, J. Magn. Reson. Imaging 8 (1) (1998) 175–181.
[23] N.R. Miller, J.C. Bamber, P.M. Meaney, Fundamental limitations of noninvasive temperature imaging by means of ultrasound echo strain estimation, Ultrasound Med. Biol. 28 (10) (2002) 1319–1333.
[24] M.J. Daniels, T. Varghese, E.L. Madsen, et al., Non-invasive ultrasound-based temperature imaging for monitoring radiofrequency heating—phantom results, Phys. Med. Biol. 52 (16) (2007) 4827.
[25] J. Yao, L.V. Wang, Photoacoustic microscopy, Laser Photonics Rev. 7 (5) (2013) 758–778.
[26] S. Cheng, Y. Zhou, J. Chen, et al., High-resolution photoacoustic microscopy with deep penetration through learning, Photoacoustics 25 (2022) 100314.
[27] W. Pang, B. Zhu, H. Li, et al., Direct monitoring of whole-brain electrodynamics via high-spatiotemporal resolution photoacoustics with voltage-sensitive dye, Laser Photonics Rev. (2024) 2400165.
[28] P. Lai, L. Wang, J.W. Tay, et al., Photoacoustically guided wavefront shaping for enhanced optical focusing in scattering media, Nat. Photonics 9 (2) (2015) 126–132.
[29] H.F. Zhang, K. Maslov, G. Stoica, et al., Functional photoacoustic microscopy for high-resolution and noninvasive in vivo imaging, Nat. Biotechnol. 24 (7) (2006) 848–851.
[30] J. Staley, P. Grogan, A.K. Samadi, et al., Growth of melanoma brain tumors monitored by photoacoustic microscopy, J. Biomed. Opt. 15 (4) (2010) 040510.
[31] J. Yao, K.I. Maslov, Y. Zhang, et al., Label-free oxygen-metabolic photoacoustic microscopy in vivo, J. Biomed. Opt. 16 (7) (2011) 076003.
[32] E.I. Galanzha, E.V. Shashkov, P.M. Spring, et al., In vivo, noninvasive, label-free detection and eradication of circulating metastatic melanoma cells using two-color photoacoustic flow cytometry with a diode laser, Cancer Res. 69 (20) (2009) 7926–7934.
[33] Y. Zhang, X. Cai, S.W. Choi, et al., Chronic label-free volumetric photoacoustic microscopy of melanoma cells in three-dimensional porous scaffolds, Biomaterials 31 (33) (2010) 8651–8658.
[34] L. Gao, L. Wang, C. Li, et al., Single-cell photoacoustic thermometry, J. Biomed. Opt. 18 (2) (2013) 026003.
[35] K.H. Song, E.W. Stein, J.A. Margenthaler, et al., Noninvasive photoacoustic identification of sentinel lymph nodes containing methylene blue in vivo in a rat model, J. Biomed. Opt. 13 (5) (2008) 054033.
[36] Y. Xu, L.V. Wang, G. Ambartsoumian, et al., Reconstructions in limited-view thermoacoustic tomography, Med. Phys. 31 (4) (2004) 724–733.
[37] L. Lin, P. Hu, J. Shi, et al., Single-breath-hold photoacoustic computed tomography of the breast, Nat. Commun. 9 (1) (2018) 1–9.
[38] Z. Yu, H. Li, P. Lai, Wavefront shaping and its application to enhance photoacoustic imaging, Appl. Sci. 7 (12) (2017) 1320.
[39] Z. Yu, H. Li, T. Zhong, et al., Wavefront shaping: a versatile tool to conquer multiple scattering in multidisciplinary fields, Innovation 3 (5) (2022).
[40] H. Li, Z. Yu, T. Zhong, et al., Performance enhancement in wavefront shaping of multiply scattered light: a review, J. Biomed. Opt. 29 (S1) (2024) S11512. S11512.

Zezheng Qin is currently pursuing his Ph.D. degree in the school of Astronautics, Harbin Institute of Technology, Harbin, China. His research interests include developing novel biomedical imaging tools based on photoacoustic imaging for preclinical and clinical applications.

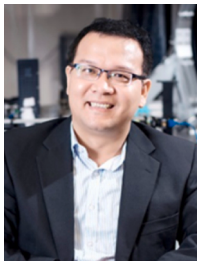

Puxiang Lai is currently an Associate Professor at the Department of Biomedical Engineering at the Hong Kong Polytechnic University. His research interests focus on deep-tissue optical focusing, imaging, stimulation, and treatment. Current research projects include, but are not limited to, wavefront shaping, photoacoustic imaging, neuron stimulation, computational optics, and artificial intelligence. His research has fueled more than 100 top journal publications, such as Nature Photonics, Nature Communications, Light: Science & Applications, PhotoniX, Advanced Photonics, Advanced Science, and The Innovation. He has been invited to give more than 100 seminars or invited talks worldwide. Dr. Lai was awarded the 2016 National (Youth) Talent Award and the 2016–2017 Hong Kong RGC Early Career Award. As a recognition for his contribution to the field, currently Puxiang serves as Associate Editor or Editor for a few premium journals, such as The Innovation, The Innovation Medicine, Advanced Photonics Nexus, Advanced Imaging, Journal of Visual Computing for Industry, Biomedicine, and Art (VCIBA), and Journal of Innovative Optics in Health and Science (JIOHS). He is also a Guest Professor of Southern Medical University (China).

Mingjian Sun is a professor at Harbin Institute of Technology, Weihai, China. He received B.E. degree from Harbin Institute of Technology in 2003, and Ph.D. degree from Harbin Institute of Technology in 2011, respectively. His main research interests include photoacoustic imaging technology, artificial intelligence medicine and its clinical translation